Hybrid Quantum-Classical Optimization for Joint Beamforming and Discrete Phase Shift Design in STAR-RIS 6G Networks

Vu Phong Pham, Dang Van Huynh, Haejoon Jung, *Senior Member, IEEE*, Berk Canberk, *Senior Member, IEEE*, Simon L. Cotton, *Fellow, IEEE*, Hyundong Shin, *Fellow, IEEE*, and Trung Q. Duong, *Fellow, IEEE*

***Abstract*—Simultaneous transmitting and reflecting reconfigurable intelligent surface (STAR-RIS) has received significant attention as a potential technology for the sixth generation (6G) of wireless network due to its ability to boost signal coverage and enhance system efficiency. In this paper, we investigate the potential of a near-optimal hybrid quantum-classical optimization approach to jointly optimize beamforming and the discrete phase shifts of the STAR-RIS assisted wireless network. In particular, we formulate a discrete optimization problem to maximize the total power transmitted to the ground users. This is achieved by optimizing the beamforming at the base station (BS) and the phase shift of the STAR-RIS under minimal power allocation for each user and the maximum power budget at the BS. Since the addressed problem is NP-hard, we propose a quantum approximate optimization algorithm with alternating optimization (QAOA-AO) method that iteratively addresses beamforming components and discrete phase shifts to search for the near-optimal solutions for the problem. Numerical results validate the effectiveness and robustness of the proposed QAOA-AO compared to the classical benchmarks in terms of runtime and system power, and highlight its potential for practical deployment when solving medium-to-large-scale networks.**

***Index Terms*—Simultaneous transmitting and reflecting reconfigurable intelligent surface (STAR-RIS), 6G networks, alternating optimization (AO), beamforming, discrete phase shift optimization, quantum approximate optimization algorithm (QAOA).**

V. P. Pham is with the Faculty of Engineering and Applied Science, Memorial University, St. John's, NL A1B 3X5, Canada (e-mail: vppham@mun.ca).

D. V. Huynh is with the Faculty of Computer Networks and Communications, University of Information Technology, Vietnam National University, Ho Chi Minh City, Quarter 34, Linh Xuan Ward, Ho Chi Minh City, Vietnam and was with Faculty of Engineering and Applied Science, Memorial University, St. John's, NL A1B 3X5, Canada (e-mail: danghv@uit.edu.vn).

H. Jung and H. Shin are with the Department of Electronics and Information Convergence Engineering, Kyung Hee University, Gyeonggi 17104, Republic of Korea (e-mail: {haejoonjung, hshin}@khu.ac.kr).

S. L. Cotton is with the Centre for Wireless Innovation (CWI), School of Electronics, Electrical Engineering and Computer Science, Queen's University Belfast, BT7 1NN Belfast, U.K. (e-mail: simon.cotton@qub.ac.uk).

B. Canberk is with the School of Computing, Engineering and Built Environment, Edinburgh Napier University, Edinburgh EH10 5DT, U.K. (e-mail: b.canberk@napier.ac.uk).

T. Q. Duong is with the Faculty of Engineering and Applied Science, Memorial University, St. John's, NL A1C 5S7, Canada, and with the School of Electronics, Electrical Engineering and Computer Science, Queen's University Belfast, Belfast, U.K, and also with the Department of Electronic Engineering, Kyung Hee University, Yongin-si, Gyeonggi-do 17104, South Korea (e-mail: tduong@mun.ca).

This paper has been accepted in part for presentation at the International Conference on Computing, Networking and Communications (ICNC 2026), Maui, Hawaii, USA, Feb 2026.

The work of T. Q. Duong was supported in part by the Canada Excellence Research Chair (CERC) Program CERC-2022-00109, in part by the Natural Sciences and Engineering Research Council of Canada (NSERC) Discovery Grant Program RGPIN-2025-04941, and in part by the NSERC CREATE program (Grant number 596205-2025). This work of H. Jung was supported in part by Institute of Information & communications Technology Planning & evaluation (IITP) grant funded by the Korea government (MSIT) (No. RS-2024-00397480, System Development of Smart Repeater in Upper-mid Band). The work of B. Canberk is partially supported by The Scientific and Technological Research Council of Türkiye (TÜBİTAK) 1515 Frontier R&D Laboratories Support Program for Türk Telekom 6G R&D Lab under project number 5249902. The work of S. L. Cotton was funded in part by the U.K. Engineering and Physical Sciences Research Council (EPSRC) through the EPSRC Hub on All Spectrum Connectivity under Grant EP/X040569/1 and Grant EP/Y037197/1. The work of H. Shin was supported in part by the National Research Foundation of Korea (NRF) grant funded by the Korean government (MSIT) (RS-2025-00556064), and by the Ministry of Science and ICT (MSIT), Korea, under the ITRC (Information Technology Research Center) support program (IITP-2025-RS-2021-II212046), supervised by the IITP (Institute for Information & Communications Technology Planning & Evaluation).

Corresponding authors are Trung Q. Duong and Hyundong Shin.

I. Introduction

The sixth-generation (6G) of mobile networks is envisioned to revolutionize connectivity by creating a cyber-physical ecosystem where the physical and digital worlds are globally converged [1], [2]. To this end, 6G must not only improve upon traditional key performance indicators (KPIs) such as capacity, coverage, speed, and latency but also introduce new performance dimensions, including availability, reliability, predictability, resilience, and trustworthiness. These advancements are crucial for supporting the projected proliferation of diverse Internet-of-Things (IoT) devices, which are anticipated to exceed 100 billion by 2030. However, achieving the ambitious goals of 6G cannot be accomplished simply by evolving existing fifth-generation (5G) technologies. Although techniques such as massive multiple-input multiple-output (MIMO), millimeter-wave (mmWave) communication [3], and ultra-dense networks (UDN) have significantly enhanced wireless performance, they possess fundamental limitations that inhibit their scalability. For example, massive MIMO achieves high spectral efficiency at the cost of substantial hardware cost and high computation complexity. While mmWave communication can provide large bandwidths, it is constrained by high sensitivity to blockages and expensive infrastructure deployment. Although UDNs improve capacity through densification, this approach introduces significant challenges with inter-cell interference, complex resource management, and stringent backhaul requirements. These limitations underscore the necessity for research into innovative technologies capable

of overcoming the inherent challenges of the 5G framework. This has motivated the exploration of new paradigms to satisfy the requirements of future use cases.

Reconfigurable intelligent surface (RIS) has recently emerged as a potential technology for 6G networks which can further enhance the spectrum and energy efficiency [1], [2], [4]–[9]. In its simplest form, a RIS is a two-dimensional programmable metasurface composed of many small unit cells such as meta atoms or simply RIS elements. These low-cost elements are engineered to individually manipulate the properties of incoming electromagnetic waves. Depending on the design, each element can primarily adjust the phase shift, and in more advanced configurations, the amplitude or polarization of the signal with minimal power consumption to reconfigure the wireless channel [5], [10]. By precisely designing the phase response of each element, a RIS can perform targeted beamforming to enhance received power, null signals for physical layer security, and actively suppress inter-user interference. Unlike conventional relays, when deployed in its passive form, a RIS contains no power-hungry radio frequency chains or amplifiers, yielding significant reductions in hardware cost and energy consumption. This efficiency enables a thin, lightweight form factor suitable for large-scale, unobtrusive deployment on available surfaces in the environment such as building walls (indoor and outdoor) and ceilings. Consequently, RIS technology is a strong candidate for overcoming the fundamental performance and efficiency challenges inherent in future 6G networks. Studies available in the literature are mainly focused on coverage [11]–[13], channel modeling [14], interference mitigation [15], [16], positioning improvement [17], or combinations with other wireless communications techniques such as integrated sensing and communication (ISAC) [18], [19], or space-air-ground integrated network (SAGIN) [20], [21]. However, due to its hardware design, conventional RIS can only reflect incident signals and support wireless devices on one side, significantly restricting its deployment flexibility and coverage area. To address this limitation, simultaneous transmitting and reflecting RIS (STAR-RIS) has emerged as a solution to this problem by enabling reflection and refraction (or transmission) of the broadcast signals through the cells. Unlike traditional RIS technology that can only serve users in the half-space, innovative STAR-RIS can provide full-space coverage, greatly enhancing network performance.

A. Literature Review and Related Works

From a physical perspective, STAR-RIS enables the reflection and transmission (or refraction) of incident signals through the RIS elements. This extensive functionality allows the RIS elements to serve users and devices using both sides of the surface and provide full coverage instead of the half-space limitation in conventional RIS. The practical implementability of STAR-RIS technology has been demonstrated using a dynamic metasurface developed by NTT DOCOMO [22]. One of the first investigations focusing on the design of STAR-RIS, its physical principles, and communication systems is reported in [23]. The advantages of STAR-RIS technology over conventional reflecting-only RIS as well as several key applications of STAR-RISs in 6G networks were highlighted [23]. Building upon the strengths of conventional RIS, STAR-RIS technology offers even greater potential to enhance the spectral and energy efficiency of next-generation mobile networks. STAR-RIS can also be used to assist mobile networks by integrating with other technologies such as non-orthogonal multiple access (NOMA), orthogonal multiple access (OMA) [13], near-field and far-field [24], ISAC [25], and SAGIN [26]. A narrow-band STAR-RIS-aided downlink communication network using the NOMA and OMA multiple access schemes was introduced in [13], where the network consisted of a single-antenna access point (AP) communicating with two single-antenna users at each side. The maximal coverage range was formed by aggregating the transmission coverage and the reflection coverage ranges. The simulation results revealed that under different conditions, such as adjusting minimum quality of service (QoS) requirements or employing a different number of RIS elements, the NOMA-STAR scheme was the superior method compared to OMA-STAR, conventional NOMA, and conventional OMA schemes. Similarly, an equivalent system model with one transmitter and two receivers on each side of the STAR-RIS, where each component was equipped with one antenna, was introduced in [24]. The objective was to compare the performance of the STAR-RIS model with that of reflecting-only RIS in the near- and far- fields to demonstrate the benefit of applying STAR-RISs in a wireless network. Their numerical results verified that the STAR-RIS can extend coverage and achieve a higher diversity order on both sides of the surface compared to conventional RIS.

The potential benefits of using STAR-RIS to support ISAC was also investigated in [25], where a dual-functional BS (DFBS) operating in full-duplex (FD) mode was used to simultaneously provide communication services to multiple users linked with a single antenna and perform target sensing. The main objective was to maximize the achievable total throughput, while satisfying the minimum radar signal-to-interference-plus-noise ratio (SINR) requirement, active STAR-RIS hardware constraints, and total power budget for DFBS and STAR-RIS. Numerical results demonstrated the performance enhancement of the sum-rate and radar SINR compared to passive STAR-RIS or non-RIS benchmarks. In [26], STAR-RIS was applied to assist train-to-ground communications with a low earth orbit satellite, a moving train and a single airship located between two BSs. The work aimed at optimizing the transmission scheduling to meet QoS requirements for flows in STAR-RIS-assisted train-to-ground communications while addressing interference and coverage gaps in SAGIN. Numerical results demonstrated the superiority of the approach over traditional algorithms in different train speeds, airship heights, QoS requirements, numbers of STAR-RIS cells, and numbers of carriages.

B. Motivation and Contributions

Despite numerous investigations into optimizing STAR-RIS-aided wireless communications, most of the work is built upon assumption that STAR-RISs elements are continuous phase shifts to modify their reflection angle and refractive

angle at high precision. In practice, this is very difficult to achieve. The implementation of STAR-RIS is extremely challenging due to the high accuracy and current hardware limitations [27]. Therefore, employing STAR-RIS with discrete phase shifts is more realistic. Another limitation is that optimal resource allocation algorithms are cost-effective, such as cross-entropy optimization along with zero-forcing beamforming [28]–[30], hybrid deep deterministic policy gradient, and joint DDPG with a deep-Q network-based algorithm. These methods are still highly complex and limited to classical computing systems, whose linear scalability with added resources makes them inefficient for problems of exponential complexity. The alternating optimization (AO) method in [28] also provided an effective direct solution for each iteration, which ensures a local optimal solution; however, the applicability of this approach is limited when extended to problems with more intricate designs and numerous constraints, which preclude the derivation of direct or approximate solutions. It is therefore clear that developing new methods capable of solving these high-complexity problems is essential for managing the increasing scale of modern communication networks.

Quantum approximate optimization algorithm (QAOA) is a promising method for addressing NP-hard mixed-integer problems (MIPs), suited for implementation on both noisy intermediate-scale quantum (NISQ) hardware and quantum simulators such as Qiskit Aer [31]–[33]. In short, QAOA is a hybrid quantum-classical approach in which the angle parameters of its quantum circuit layers are iteratively optimized using a classical computer, while the solution is derived from the measurement outcomes of the QAOA circuit executed on a quantum computer. Several studies on QAOA have verified its validity and robustness in different use cases such as vehicle routing [34], electric vehicle charging [35], satellite mission planning [36], supply chain [37] and edge computing [38]. These findings provide strong evidence that quantum optimization is a promising approach for a wide range of applications, notably in STAR-RIS technology and next-generation mobile networks.

Motivated by the aforementioned works, this paper introduces a hybrid QAOA-AO method to address the joint beamforming and discrete phase shift design in STAR-RIS-assisted wireless network. The contributions of this work are summarized as follows:

- We formulate a comprehensive problem for maximizing the sum received signal power by jointly optimizing the BS beamforming and the STAR-RIS discrete phase shifts, while satisfying the maximum transmit power at the BS and the minimum power allocation for each user. In addition, the system model considers different quantization levels of the STAR-RIS phase shift to further examine the improvement of total transmit signals compared to the quantum bits (qubits) used in the algorithm.
- To tackle this problem, we split the considered problem into two subproblems, where either a set of beamforming variables or discrete phase shifts is fixed and the aim is to optimize the other set. The phase shifts subproblem is addressed by reformulating the considered objective function into a quadratic unconstrained binary optimization (QUBO) form and solving it using a quantum simulator, whereas the beamforming subproblem is solved by utilizing the Rayleigh quotient solution and balancing the beamforming amplitude based on the minimum power constraint.
- After deriving separate methodologies to solve each subproblem, an AO algorithm is proposed to iteratively solve for each variable set and automatically updated after each iteration, until the convergence condition is reached.
- We validate the effectiveness and robustness of the proposed QAOA-AO framework through comprehensive numerical simulations. The results demonstrate two key advantages: our framework significantly enhances the total power delivered to users compared to benchmark schemes, and it achieves optimal solutions that match those found via a Brute-Force search.

Previously, an equivalent system model was studied in [7], [28]; however, the system model uses multi-antenna BS to serve only one single-antenna user and did not consider the minimum power allocation for each user. In addition, the algorithms used in these works are based only on classical computing, which is challenging and inefficient when the number of antennas utilized in the BS or the elements in STAR-RIS grows exponentially. Different from these works, this paper aims to propose a hybrid QAOA-AO algorithm to make use of quantum computing and iteratively maximize the total received power to users.

The remainder of this paper is organized as follows. Section II introduces the system model and formulates the joint optimization problem for two distinct cases of phase shift quantization. Section III then proposes a detailed QUBO-AO methodology to solve the first case, featuring two-level phase shifts. This algorithm is extended in Section IV to address the more complex four-level quantization case. In Section V, we present and analyze the performance of our framework through extensive Monte Carlo simulations. Finally, Section VI concludes the paper with a summary of our key contributions and directions for future research.

Notations: Throughout the paper, numbers are represented by lowercase letters, while matrices and vectors are denoted by bold uppercase and lowercase letters, respectively. For example, $\mathbf{\Theta}$, $\mathbf{v}$ are used to describe the vectors and matrices of variables, while regular letters such as $h_{i,pm}^{H}$ or p are given parameters or a specific variable in the vectors of variables. $\|.\|$ and $|.|$ denote the Euclidean norm of a vector or a matrix, and the absolute value of a scalar. $x \sim \mathcal{CN}(\mu, \sigma)$ means that x is a scalar that follows the complex Gaussian distribution with mean μ and covariance σ. $\Re\{.\}$ and $\Im\{.\}$ denote the real and imaginary parts of the arguments, respectively.

II. System Model and Problem Formulation

A. System Model

In this study, we consider a STAR-RIS-aided downlink (DL) wireless system, as shown in Fig. 1. Herein, a terrestrial M-antenna BS is used to transmit the desired signals to N terrestrial single-antenna users with the help of a STAR-RIS implemented as an active beamforming relay to transmit

TABLE I: Summary of Notations

Symbol	Description
M	Number of antennas attached in BS.
N	Number of users in the communication network.
P	Number of STAR-RIS reflecting elements.
Q	Number of bits used to discretize the phase shifts.
$\mathcal{D}_Q$	Set of eligible discrete phase shifts in STAR-RIS.
$\mathcal{M}$	Set of index from 1 to M.
$\mathcal{N}$	Set of index from 1 to N.
$\mathcal{P}$	Set of index from 1 to P.
φ_i	Path loss exponent from the BS to the STAR-RIS.
φ_r	Path loss exponent from the STAR-RIS to users.
φ_d	Path loss exponent from the BS to users.
$\tilde{h}$	Rayleigh small-scale fading.
$\mathbf{h_{i,p}^H}$	Channel coefficient vector from the p-th element to the STAR-RIS.
$\mathbf{H_I^H}$	Matrix of channel coefficients from the BS to the STAR-RIS.
$\mathbf{h_{r,n}^H}$	Channel coefficient vector from the STAR-RIS to the n-th user.
$\mathbf{h_{d,n}^H}$	Channel coefficient vector from the BS to the n-th user.
$\boldsymbol{\theta}$	Set of phase shifts of the STAR-RIS reflecting elements.
$\mathbf{x}$	The complex signal broadcasted by the BS.
$\mathbf{w}_n$	The beamforming vector headed to user n.
s_n	Signal broadcasted to user n.
z_n	The additive white Gaussian noise with zero mean and variance σ^2.
$\mathbf{w}$	Set of beamforming vectors towards all users from the BS

signals to users. Hence, the communications between the BS and users consist of the direct link and STAR-RIS-reflected transmission link. The number of reflecting elements of the STAR-RIS is set as P. The set of these on-ground users, BS antennas, and reflecting elements can now be denoted as $\mathcal{N} \triangleq \{1,\ldots,N\}$, $\mathcal{M} \triangleq \{1,\ldots,M\}$, and $\mathcal{P} \triangleq \{1,\ldots,P\}$, respectively.

Let us denote $h_{i,pm}^H \in \mathbb{C}$ as the channel coefficient of the antenna $m \in \mathcal{M}$ to the STAR-RIS element $p \in \mathcal{P}$, $\mathbf{h_{i,p}^H} \triangleq \{h_{i,pm}^H\}_{m\in\mathcal{M}} \in \mathbf{C}^{1\times M}$ and $\mathbf{H_I^H} \triangleq \{\mathbf{h_{i,p}^H}\} \in \mathbb{C}^{P\times M}$ as the channel gain vector coming from the element p and the matrix of channel coefficients from the BS to the STAR-RIS, respectively. Similarly, $h_{r,np}^H \in \mathbb{C}$ is defined as the channel gain from the reflecting element $p \in \mathcal{P}$ to the user $n \in \mathcal{N}$, and $\mathbf{h_{r,n}^H} \triangleq \{h_{r,np}^H\} \in \mathbb{C}^{1\times P}$ denotes the channel gain vector from the STAR-RIS to user n. The channel gain of the direct DL from antenna $m \in \mathcal{M}$ to user $n \in \mathcal{N}$ can be assigned as $h_{d,nm}^H$, and $\mathbf{h_{d,n}^H} \triangleq \{h_{d,nm}^H\} \in \mathbb{C}^{1\times M}$.

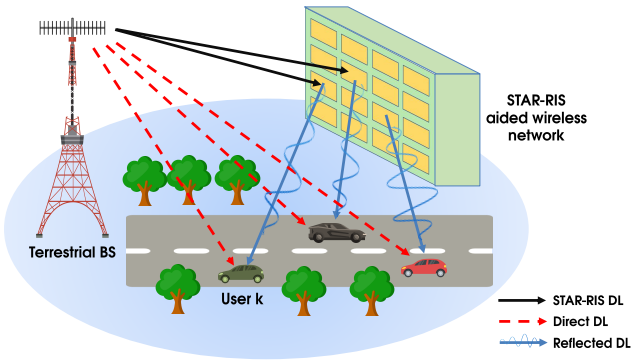

Fig. 1: An illustration of a simultaneous transmitting and reflecting reconfigurable intelligent surface (STAR-RIS) deployed in downlink communication system to enhance the wireless network and signal quality.

Due to the complex propagation environment with multi-path and arbitrary motions of the users, both direct and STAR-RIS-reflected transmission channels follow the independent small-scale Rayleigh fading. In other words, the channel coefficient between components p and q can be written as $h_{X,pq}^H = d_{X,pq}^{-\varphi_X/2}\tilde{h}$, where $\varphi_i, \varphi_d, \varphi_r$ denote the path loss exponent in the STAR-RIS DL, direct DL and reflected DL, respectively. $\tilde{h}$ is the Rayleigh small-scale fading, i.e., $\tilde{h} \sim \mathcal{CN}(0,1)$, and the subscript $X \in \{i,r,d\}$ is used to distinguish channel categories. $d_{X,pq}$ is the Euclidean distance between p and q.

Let $\boldsymbol{\theta} \triangleq [\theta_1,\ldots,\theta_P]$ be the set of phase shifts of the reflecting elements in the STAR-RIS. It is known that the interference power can be steadily reduced by merely modifying the phase shifts of the STAR-RIS elements [39], so we set the amplitude of these elements equals to 1. Furthermore, the phase shift θ_p of the STAR-RIS is also restricted to $\theta_p \in \mathcal{D}_Q \triangleq \left\{\frac{2\pi(q-1)}{2^Q}\right\}$, where Q is the number of bits used to discretize the phase shifts and $q = 1,\ldots,2^Q$. Let $\boldsymbol{\Theta} = \text{diag}\left\{e^{j\theta_1},\ldots,e^{j\theta_P}\right\}$ be the parameters that characterize the way STAR-RIS elements modify the original transmitted signal wave.

The complex transmitted signal broadcasted by the BS can be expressed as $\mathbf{x} = \sum_{n\in\mathcal{N}} \mathbf{w}_n s_n$, where s_n represents the signal needed to transfer to user n and $\mathbf{w}_n \triangleq \{\mathrm{w}_{nm}\} \in \mathbb{C}^{M\times 1}$ is the associated beamforming vector. It is also assumed that the transmitted signals $s_n, \forall n \in \mathcal{N}$ are independent and identically distributed random variables with zero mean and unit variance. Now, the signal transmitted from the terrestrial BS to user n can be written as

$$\begin{aligned} y_n &= y_n^d + y_n^r \\ &= \mathbf{h_{d,n}^H x} + \mathbf{h_{r,n}^H \Theta H_I^H x} + z_n \\ &= \left(\mathbf{h_{d,n}^H} + \mathbf{h_{r,n}^H \Theta H_I^H}\right) \sum_{n\in\mathcal{N}} \mathbf{w_n} s_n + z_n, \end{aligned} \tag{1}$$

where z_n is the additive white Gaussian noise (AWGN) with zero mean and variance σ^2.

B. Optimization Problem Formulation

In this paper, we focus on maximizing the total received signal power by jointly optimizing the beamforming of the BS $\mathbf{w}$, and discrete phase shifts of STAR-RIS $\boldsymbol{\theta}$. The problem of jointly optimizing beamforming and RIS phase shift to maximize total powers received by users has been investigated by [7]. In our system, maximizing the total received signal power directly captures the quality of signal delivery from the BS to the users through both the direct and STAR-RIS-assisted links. This objective also serves as a tractable system-level metric for evaluating and improving the proposed design. However, this problem mainly focused on optimizing the continuous STAR-RIS phase shift. In contrast, we consider the discrete phase shift for STAR-RIS, which is easier to implement and lower cost. Due to hardware limitations and restricted number of qubits, we propose a hybrid quantum-classical solution for the small number of discrete phase shifts, e.g.,, this paper only studies two main cases as $Q = 1$ and $Q = 2$. By denoting $\mathbf{w} \triangleq \{\mathbf{w_n}\}_{n\in\mathcal{N}}$, the total superimposed signal optimization problem can be fully expressed as follows:

$$\max_{\mathbf{w},\boldsymbol{\theta}} \sum_{n\in\mathcal{N}} \left|\left(\mathbf{h_{d,n}^H} + \mathbf{h_{r,n}^H}\boldsymbol{\Theta}\mathbf{H_I^H}\right)\mathbf{w_n}\right|^2, \tag{2a}$$

$$\text{s.t. } \|\mathbf{w}\|^2 \le P_{\max}, \tag{2b}$$

$$\|\mathbf{w_n}\|^2 \ge P_{\min}, \forall n \in \mathcal{N}, \tag{2c}$$

$$\theta_p \in \mathcal{D}_Q, \forall p \in \mathcal{P}. \tag{2d}$$

In the above problem, the objective (2a) maximizes the total signal power of the ground users. The first constraint (2b) limits the maximum transmitted power of the BS, and the second constraint (2c) ensures that the BS allocates the transmission power to each user and the minimum power must not be lower than $P_{\min}$. Finally, constraint (2d) represents the discrete variables θ_p.

III. Proposed QAOA solution for the total signal power maximization problem in the case of $Q = 1$

Note that the maximum value of the objective can only be reached when the equality of constraint (2b) is satisfied, i.e., $\|\mathbf{w}\| = P_{\max}$ because of the scalability [40]. Therefore, the primary problem can be reconstructed as follows:

$$\max_{\mathbf{w},\boldsymbol{\theta}} \sum_{n\in\mathcal{N}} \left|\left(\mathbf{h_{d,n}^H} + \mathbf{h_{r,n}^H}\boldsymbol{\Theta}\mathbf{H_I^H}\right)\mathbf{w_n}\right|^2, \tag{3a}$$

$$\text{s.t. } \|\mathbf{w}\|^2 = P_{\max}, \tag{3b}$$

$$\|\mathbf{w_n}\|^2 \ge P_{\min}, \forall n \in \mathcal{N}. \tag{3c}$$

$$\theta_p \in \mathcal{D}_1, \forall p \in \mathcal{P}. \tag{3d}$$

Herein, $\mathcal{D}_1 = \{0, \pi\}$. Although we have restricted our attention to the small discrete phase shift ($Q = 1$), the optimization problem is still difficult to solve due to the discrete variables $\boldsymbol{\theta}$. Moreover, the problem is NP-hard, i.e., extremely challenging and time-consuming to find the optimal value computationally. Hence, to tackle this optimization problem, we first apply the AO algorithm to divide the original problem into two subproblems. Each subproblem will have a subset of fixed variables and we only need to optimize the remaining ones. Specifically, considering the subproblem where the beamforming power $\mathbf{w}$ is fixed, we will try to convert the terms related to $\boldsymbol{\theta}$ to expressions of binary variables. Then, this subproblem will be transformed into a Hamiltonian formulation which can be efficiently solved by the QAOA approach via quantum processor. For the subproblem with the STAR-RIS elements being fixed, we obtain the optimal beamforming power directly due to the quadratic form of the objective.

A. Phase Shift Optimization Subproblem

To formulate this subproblem, let us first set $\mathbf{w} = \mathbf{w^{(t)}} \triangleq \{\mathbf{w}_n^{(t)}\}$, which is a feasible solution of (3). We also denote $P_{T,\boldsymbol{\theta}}^{(t)}(\boldsymbol{\theta}) \triangleq \sum_{n\in\mathcal{N}} \left|\left(\mathbf{h_{d,n}^H} + \mathbf{h_{r,n}^H}\boldsymbol{\Theta}\mathbf{H_I^H}\right)\mathbf{w}_n^{(t)}\right|^2$. From these denotations, we reformulate the subproblem as

$$\max_{\boldsymbol{\theta}} \; P_{T,\boldsymbol{\theta}}^{(t)}(\boldsymbol{\theta}), \tag{4a}$$

$$\text{s.t. } \theta_p \in \mathcal{D}_1, \forall p \in \mathcal{P}. \tag{4b}$$

This subproblem is a discrete optimization problem with the discrete variable $\boldsymbol{\theta}$. To achieve the Hamiltonian formulation, we first need to reformulate this subproblem into a QUBO expression. Generally, a QUBO problem can be described as

$$\min_{\mathbf{x}} \; \mathbf{x^T Q x}, \tag{5a}$$

$$\text{s.t. } x_i \in \{0, 1\}, \forall x_i \in \mathbf{x}. \tag{5b}$$

In this general form, $\mathbf{x} \in \{0, 1\}^n$ is the binary vector and $\mathbf{Q} \in \mathbb{R}^{n\times n}$ is a symmetric matrix that describes the linear terms of the variables in $\mathbf{x}$ and the interactions between two different decision variables in $\mathbf{x}$. Since our subproblem is the maximization problem, we first convert it into a minimization problem as

$$\min_{\boldsymbol{\theta}} \; -P_{T,\boldsymbol{\theta}}^{(t)}(\boldsymbol{\theta}), \tag{6a}$$

$$\text{s.t. } \theta_p \in \mathcal{D}_1, \forall p \in \mathcal{P}. \tag{6b}$$

To simplify the objective in (6a), $P_{T,\boldsymbol{\theta}}^{(t)}(\boldsymbol{\theta})$ can be separated as the sum of the signal power components as follows:

$$\begin{aligned} &-P_{T,\boldsymbol{\theta}}^{(t)}(\boldsymbol{\theta}) \\ &= -\sum_{n\in\mathcal{N}} \left|\sum_{m\in\mathcal{M}} \left(h_{d,nm}^H + \sum_{p\in\mathcal{P}} h_{r,np}^H e^{j\theta_p} h_{i,pm}^H\right) \mathrm{w}_{nm}^{(t)}\right|^2 \\ &\triangleq -\sum_{n\in\mathcal{N}} Q_{n,\boldsymbol{\theta}}^{(t)}(\boldsymbol{\theta}), \end{aligned} \tag{7}$$

It is worth noting that $e^{j\theta_p} = \cos\theta_p$ since $\sin\theta_p$ is always equal to 0. Following this, by defining $T_{nm}^{r,(t)} \triangleq \Re\{h_{d,nm}^H \mathrm{w}_{nm}^{(t)}\}, T_{nm}^{i,(t)} \triangleq \Im\{h_{d,nm}^H \mathrm{w}_{nm}^{(t)}\}$ and $S_{p,nm}^{r,(t)} \triangleq \Re\{h_{r,np}^H h_{i,pm}^H \mathrm{w}_{nm}^{(t)}\}, S_{p,nm}^{i,(t)} \triangleq \Im\{h_{r,np}^H h_{i,pm}^H \mathrm{w}_{nm}^{(t)}\}, \forall n \in \mathcal{N}$, we can rewrite $Q_{n,\boldsymbol{\theta}}^{(t)}(\boldsymbol{\theta})$ as

$$Q_{n,\boldsymbol{\theta}}^{(t)}(\boldsymbol{\theta}) = \Bigg| \sum_{m\in\mathcal{M}} \sum_{p\in\mathcal{P}} (S_{p,nm}^{r,(t)} + jS_{p,nm}^{i,(t)}) \cos\theta_p + \sum_{m\in\mathcal{M}} (T_{nm}^{r,(t)} + jT_{nm}^{i,(t)}) \Bigg|^2$$
$$= \Bigg[\Bigg(\sum_{m\in\mathcal{M}} T_{nm}^{i,(t)} + \sum_{m\in\mathcal{M}} \sum_{p\in\mathcal{P}} S_{p,nm}^{i,(t)} \cos\theta_p \Bigg)^2 + \Bigg(\sum_{m\in\mathcal{M}} T_{nm}^{r,(t)} + \sum_{m\in\mathcal{M}} \sum_{p\in\mathcal{P}} S_{p,nm}^{r,(t)} \cos\theta_p \Bigg)^2 \Bigg]. \quad (8)$$

Then, we denote $\mathcal{T}_n^{r,(t)} \triangleq \sum_{m\in\mathcal{M}} T_{nm}^{r,(t)}, \mathcal{T}_n^{i,(t)} \triangleq \sum_{m\in\mathcal{M}} T_{nm}^{i,(t)}$, and $\mathcal{S}_{p,n}^{r,(t)} \triangleq \sum_{m\in\mathcal{M}} S_{p,nm}^{r,(t)}, \mathcal{S}_{p,n}^{i,(t)} \triangleq \sum_{m\in\mathcal{M}} S_{p,nm}^{i,(t)}$, $Q_{n,\boldsymbol{\theta}}^{(t)}(\boldsymbol{\theta})$ can be rewritten as

$$Q_{n,\boldsymbol{\theta}}^{(t)}(\boldsymbol{\theta}) = (\mathcal{T}_n^{r,(t)})^2 + (\mathcal{T}_n^{i,(t)})^2 + \sum_{p\in\mathcal{P}} \left[(\mathcal{S}_{p,n}^{r,(t)})^2 + (\mathcal{S}_{p,n}^{i,(t)})^2 \right] + 2\sum_{p\in\mathcal{P}} \cos\theta_p (\mathcal{S}_{p,n}^{i,(t)} \mathcal{T}_n^{i,(t)} + \mathcal{S}_{p,n}^{r,(t)} \mathcal{T}_n^{r,(t)}) + \sum_{\substack{p,q\in\mathcal{P} \\ p\neq q}} \cos\theta_p \cos\theta_q (\mathcal{S}_{p,n}^{r,(t)} \mathcal{S}_{q,n}^{r,(t)} + \mathcal{S}_{p,n}^{i,(t)} \mathcal{S}_{q,n}^{i,(t)}). \quad (9)$$

This formulation can be attained due to the fact that $\cos^2\theta_p = 1, \forall\theta_p \in \mathcal{D}_1$. Since $\cos\theta_p \in \{1,-1\}, \forall\theta_p \in \mathcal{D}_1$, we can introduce a binary variable $a_p \in \{0,1\}$ to express θ_p as $\theta_p = a_p\pi$. We can also represent the term $\cos\theta_p$ as

$$\cos(a_p\pi) = 1 - 2a_p. \quad (10)$$

By utilizing (10), (9) can be reformulated as

$$Q_{n,\boldsymbol{\theta}}^{(t)}(\boldsymbol{\theta}) = \sum_{p\in\mathcal{P}} a_p \left(-4\mathcal{A}_{p,n}^{(t)} - 4\sum_{q\neq p} \mathcal{B}_{pq,n}^{(t)} \right) + 4 \sum_{\substack{p,q\in\mathcal{P} \\ p\neq q}} a_p a_q \mathcal{B}_{pq,n}^{(t)} + \mathcal{C}_n^{(t)}. \quad (11)$$

In this expression, the auxiliary terms $\mathcal{A}_{p,n}^{(t)}, \mathcal{B}_{pq,n}^{(t)}$ and $\mathcal{C}_n^{(t)}$ can be expressed as follows:

$$\mathcal{A}_{p,n}^{(t)} \triangleq \mathcal{S}_{p,n}^{i,(t)} \mathcal{T}_n^{i,(t)} + \mathcal{S}_{p,n}^{r,(t)} \mathcal{T}_n^{r,(t)},$$
$$\mathcal{B}_{pq,n}^{(t)} \triangleq \mathcal{S}_{p,n}^{r,(t)} \mathcal{S}_{q,n}^{r,(t)} + \mathcal{S}_{p,n}^{i,(t)} \mathcal{S}_{q,n}^{i,(t)},$$
$$\mathcal{C}_n^{(t)} \triangleq (\mathcal{T}_n^{r,(t)})^2 + (\mathcal{T}_n^{i,(t)})^2 + \sum_{p\in\mathcal{P}} \left[(\mathcal{S}_{p,n}^{r,(t)})^2 + (\mathcal{S}_{p,n}^{i,(t)})^2 \right] + 2\sum_{p\in\mathcal{P}} \mathcal{A}_{p,n}^{(t)} + \sum_{\substack{p,q\in\mathcal{P} \\ p\neq q}} \mathcal{B}_{pq,n}^{(t)}. \quad (12)$$

Next, to formulate our QUBO expression of $-P_{T,\boldsymbol{\theta}}^{(t)}(\boldsymbol{\theta})$, we use the equation (7) and remove the constant terms $\mathcal{C}_n^{(t)}$ in each term $Q_{n,\boldsymbol{\theta}}^{(t)}(\boldsymbol{\theta})$. The QUBO expression of the objective can be formulated by (7) as follows:

$$\mathcal{P}_{\text{QUBO}}^{(t)} \triangleq \sum_{p\in\mathcal{P}} a_p \sum_{n\in\mathcal{N}} \left(4\mathcal{A}_{p,n}^{(t)} + 4\sum_{q\neq p} \mathcal{B}_{pq,n}^{(t)} \right) - 4 \sum_{\substack{p,q\in\mathcal{P} \\ p\neq q}} a_p a_q \sum_{n\in\mathcal{N}} \mathcal{B}_{pq,n}^{(t)} \quad (13)$$

The formulation in (13) has now been converted to a QUBO structure with binary vector $\mathbf{a} \triangleq \{a_p\}_{p\in\mathcal{P}}$ and our coefficient matrix $\mathbf{Q}$ can be expressed as

$$Q_{pp} = \sum_{n\in\mathcal{N}} \left(4\mathcal{A}_{p,n}^{(t)} + 4\sum_{q\neq p} \mathcal{B}_{pq,n}^{(t)} \right), \forall p \in \mathcal{P},$$
$$Q_{pq} = -4 \sum_{n\in\mathcal{N}} \mathcal{B}_{pq,n}^{(t)}, \forall p,q \in \mathcal{P}, p \neq q, \quad (14)$$

where Q_{pq} is the component of $\mathbf{Q}$ in row p and column q. The next step of the process is to convert the QUBO problem in (14) into the Hamiltonian expression. To do this, spin variables $z_p = 1 - 2a_p$ are introduced and for every $p \in \mathcal{P}$, the binary decision variables a_p are converted to z_p by the equation given as

$$a_p = \frac{1 - z_p}{2}. \quad (15)$$

Based on the expressions developed above, we implement our Hamiltonian by substituting (15) into (13) and terminating the constant term as

$$H_{\text{state}}^{(t)} \triangleq -2 \sum_{p\in\mathcal{P}} z_p \sum_{n\in\mathcal{N}} \mathcal{A}_{p,n}^{(t)} - \sum_{\substack{p,q\in\mathcal{P} \\ p\neq q}} z_p z_q \sum_{n\in\mathcal{N}} \mathcal{B}_{pq,n}^{(t)}. \quad (16)$$

Following from this, we propose a QAOA-based optimization

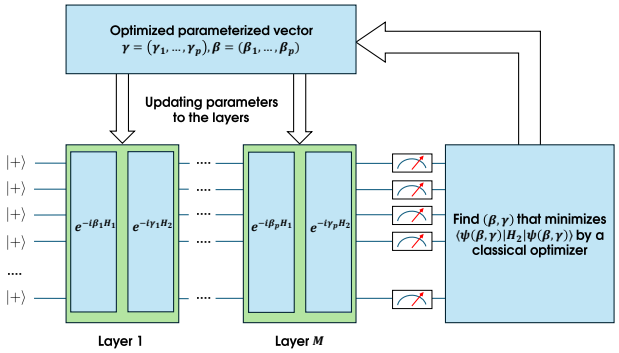

Fig. 2: An illustration of a QAOA circuit starts with an initial Hamiltonian state H_1 to the desired state H_2. The parameters are then updated until the convergence condition is held.

algorithm to tackle this problem, as illustrated in Algorithm 1. The algorithm starts by initializing some parameters that are required for the algorithm, i.e. the known parameters in the mathematical model, feasible $\mathbf{w}^{(\mathbf{t})}$ for the system, and appropriate quantum backend specifications. Subsequently, a parameterized quantum circuit (ansatz) is designed due to the known Hamiltonian objective and M_Q layers for measurements. For simplicity, we use $H_1 = \sum_i X_i$ with ground state

$|+\rangle^{\otimes N}$, while our target Hamiltonian is $H_2 = H_{\text{state}}^{(t)}$. Since QAOA is inspired by the Quantum Adiabatic Theorem, the initial state $|+\rangle^{\otimes N}$ will be converted to the ground state of H_2 by the updated layers for each QAOA iteration. For each layer m_Q, we set an initial parameter vector $(\beta_{m_Q}, \gamma_{m_Q})$ and set $(\boldsymbol{\beta}, \boldsymbol{\gamma}) \triangleq (\beta_{m_Q}, \gamma_{m_Q})_{m_Q=1,2,\ldots,M_Q}$. Then, a classical optimizer, such as COBYLA, is deployed to minimize the objective value with respect to the variational parameters $(\boldsymbol{\beta}, \boldsymbol{\gamma})$. Afterwards, the algorithm optimizes and updates the parameters iteratively until the convergence condition expressed in 1, or reaches the maximum number of iterations.

Algorithm 1 : Proposed quantum-centric optimization approach for solving the fixed-phase-shift subproblem.

1: **Input**: Required parameters $M, N, P, \mathbf{H_I^H}, \mathbf{h_{r,n}^H}, \mathbf{h_{d,n}^H}$, $\varphi, \tilde{h}, \sigma$, T_{max}, locations of network components in the system model; feasible $\mathbf{w}^{(t)}$, quantum backend settings; classical optimizer.
2: Build a parameterized ansatz circuit with M layers and an initial vector $(\boldsymbol{\beta}, \boldsymbol{\gamma})$.
3: Exploit a classical optimizer for optimizing and updating parameters iteratively.
4: Insert the parameterized vector $(\boldsymbol{\beta}, \boldsymbol{\gamma})$ into the ansatz circuit.
5: **repeat**
6: Optimize and update $(\boldsymbol{\beta}, \boldsymbol{\gamma})$ by the optimizer chosen in Step 3
7: Measure the expectation value of the quantum state $H_{\min}^{(t)} \triangleq \left\langle \boldsymbol{\beta}, \boldsymbol{\gamma} | H_{\text{state}}^{(t)} | \boldsymbol{\beta}, \boldsymbol{\gamma} \right\rangle$ and seek for convergence.
8: **until** $|H_{\min}^{(t+1)} - H_{\min}^{(t)}| < \varepsilon_{\text{tol}}$
9: **Output:** Optimized STAR-RIS phase shifts $\boldsymbol{\theta}^{(t+1)}$ constructed by binary variables and the optimal value of the objective $P_{T,\boldsymbol{\theta}}^{(t+1)}(\boldsymbol{\theta}^{(t+1)})$.

B. Beamforming Optimization Subproblem

This subproblem is created by optimizing the BS beamforming factor $\mathbf{w}$ while $\boldsymbol{\theta} = \boldsymbol{\theta}^{(t)}$ remains constant. Let us first denote $\boldsymbol{\Theta}^{(t)} \triangleq \text{diag}\left\{e^{j\theta_1^{(t)}}, \ldots, e^{j\theta_P^{(t)}}\right\}$ and $P_{T,\mathbf{w}}^{(t)}(\mathbf{w}) \triangleq \sum_{n\in\mathcal{N}} \left| \left(\mathbf{h_{d,n}^H} + \mathbf{h_{r,n}^H}\boldsymbol{\Theta}^{(t)}\mathbf{H_I^H}\right)\mathbf{w}_n \right|^2$. The problem can now be formulated as

$$\max_{\mathbf{w}} \; P_{T,\mathbf{w}}^{(t)}(\mathbf{w}), \tag{17a}$$

$$\text{s.t. } \|\mathbf{w}\|^2 = P_{\max}. \tag{17b}$$

$$\|\mathbf{w_n}\|^2 \geq P_{\min}, \forall n \in \mathcal{N}. \tag{17c}$$

In order to simplify the problem given above, let us denote $\left(\mathbf{v_n^H}\right)^{(t)} \triangleq \mathbf{h_{d,n}^H} + \mathbf{h_{r,n}^H}\boldsymbol{\Theta}^{(t)}\mathbf{H_I^H}$ and $\mathbf{v_n^{(t)}} \triangleq (\mathbf{h_{d,n}^H} + \mathbf{h_{r,n}^H}\boldsymbol{\Theta}^{(t)}\mathbf{H_I^H})^{\mathbf{H}} \in \mathbb{C}^{M\times 1}$. We also rewrite $\mathbf{w_n} = \alpha_n \mathbf{p_n}$, where α_n is the beamforming amplitude and $\mathbf{p_n}$ denotes the beamforming direction of $\mathbf{w_n}$. These beamforming factors must follow the constraint (17b) and can be rewritten as

$$\sum_{n\in\mathcal{N}} \alpha_n^2 = P_{\max}, \tag{18a}$$

$$\alpha_n^2 \geq P_{\min}, \tag{18b}$$

$$\|\mathbf{p_n}\| = 1. \tag{18c}$$

Using these expressions, the objective $P_{T,\mathbf{w}}^{(t)}(\mathbf{w})$ can be rewritten as

$$\begin{aligned} P_{T,\mathbf{w}}^{(t)}(\mathbf{w}) &= \sum_{n\in\mathcal{N}} |\left(\mathbf{v_n^H}\right)^{(t)}\mathbf{w_n}|^2 \\ &= \sum_{n\in\mathcal{N}} \mathbf{w_n^H}(\mathbf{v_n})^{(t)}\left(\mathbf{v_n^H}\right)^{(t)}\mathbf{w_n} \\ &= \sum_{n\in\mathcal{N}} \alpha_n^2 \mathbf{p_n^H}\left((\mathbf{v_n})^{(t)}\left(\mathbf{v_n^H}\right)^{(t)}\right)\mathbf{p_n} \\ &= \sum_{n\in\mathcal{N}} \alpha_n^2 \mathbf{p_n^H}\mathbf{V_n^{(t)}}\mathbf{p_n}, \end{aligned} \tag{19}$$

where, $\mathbf{V_n^{(t)}} \triangleq (\mathbf{v_n})^{(t)}\left(\mathbf{v_n^H}\right)^{(t)} \in \mathbb{C}^{M\times M}$. For constant α_n, it can be seen that maximizing $\mathbf{p_n^H}\mathbf{V_n^{(t)}}\mathbf{p_n}$ is equivalent to the Rayleigh quotient maximization problem because of (18c) and the fact that $\mathbf{V_n^{(t)}}$ is a Hermitian matrix. According to [41], the maximum value of (19) is $P_{\max}\lambda_{\max}^{n,(t)}$ and can be achieved at $\mathbf{p_n} = \mathbf{q}_{\max}^{n,(t)}$, where $\lambda_{\max}^{n,(t)}$ is the largest eigenvalue of the matrix $\mathbf{V_n^{(t)}}$ and $\mathbf{q}_{\max}^{n,(t)}$ is the corresponding eigenvector of $\mathbf{V_n^{(t)}}$.

The other factor we need to optimize is the beamforming amplitude α_n. From (18a) and (18b), the beamforming amplitude can always be bounded as

$$\sqrt{P_{\min}} \leq \alpha_n \leq \sqrt{P_{\max} - (N-1)P_{\min}}. \tag{20}$$

We now denote $j = \arg\max_{n\in\mathcal{N}}\{\lambda_{\max}^{n,(t)}\}$, which means that $\lambda_{\max}^{j,(t)} \geq \lambda_{\max}^{n,(t)}, \forall n \in \mathcal{N}$. Hence, we have the following inequality demonstrated as

$$\begin{aligned} P_{T,\mathbf{w}}^{(t)} &\leq \sum_{n\in\mathcal{N}} \alpha_n^2 \lambda_{\max}^{n,(t)} \\ &\leq (P_{\max} - (N-1)P_{\min})\lambda_{\max}^{j,(t)} + \sum_{\substack{n\in\mathcal{N} \\ n\neq j}} P_{min}\lambda_{\max}^{n,(t)}. \end{aligned} \tag{21}$$

The equality holds if and only if $\alpha_n = \sqrt{P_{\min}} = \alpha_n^{(t)}, \forall n \neq j$ and $\alpha_j = \sqrt{P_{\max} - (N-1)P_{\min}} = \alpha_j^{(t)}$. Hence, the maximizer $\mathbf{w}$ of the subproblem (17) can now be formulated as

$$\mathbf{w_n^{(t+1)}} = \alpha_n^{(t)}\mathbf{q}_{\max}^{n,(t)}, \forall n \in \mathcal{N}. \tag{22}$$

The problem of finding the maximum eigenvalue $\lambda_{\max}^{n,(t)}$ and the associated eigenvector $\mathbf{q}_{\max}^{n,(t)}$ of $\mathbf{V_n^{(t)}}$ can be directly solved thanks to available packages.

C. Proposed QAOA-AO Algorithm

Denote $P_T(\mathbf{w}, \boldsymbol{\theta}) \triangleq \sum_{n\in\mathcal{N}} \left| \left(\mathbf{h_{d,n}^H} + \mathbf{h_{r,n}^H}\boldsymbol{\Theta}\mathbf{H_I^H}\right)\mathbf{w_n} \right|^2$ and suppose $P_T^{(t)} \triangleq P_T(\mathbf{w}^{(t)}, \boldsymbol{\theta}^{(t)})$ is the maximum value of (2) at iteration t. Throughout the subproblems developed

in Sections III-A and III-B, the discrete optimization problem in (2) can be iteratively solved by using the proposed AO method as shown in Algorithm 2. The algorithm starts by initializing feasible solutions of (2) as $\boldsymbol{\theta}^{(0)}, \mathbf{w}^{(0)}$, setting $t = 0$ and some appropriate parameters given in Algorithm 1. Then, from Algorithm 1, we derive the new optimized phase shifts $\boldsymbol{\theta}^{(t+1)}$ and update $\boldsymbol{\Theta}^{(t+1)}, P_{T,\mathbf{w}}^{(t)}$. The maximizer of the following subsection $\mathbf{w}^{(t+1)}$ can be obtained from the developments in the next Section III-B and the objective can be updated as $P_T^{(t+1)}$. The counting index is then updated as $t = t + 1$ and the AO algorithm continues to operate until the convergence is reached.

Algorithm 2 : Proposed AO Algorithm for solving (2).

1: **Initialization**: Set $t = 0$, maximum number of iteration, $N_{\max}$; generate the initial feasible points $\boldsymbol{\theta}^{(0)}$ with the corresponding optimized $\mathbf{w}^{(0)}$ derived in Section III-B, and choose the known parameters in Algorithm 1.
2: **while** $P_T^{(t)} = P_T^{(t-1)}$or $t > N_{\max}$ **do**
3: Follow the developments in Section III-B and use (22) to find the optimal beamforming vectors of the BS $\mathbf{w}^{(t+1)}$ from the STAR-RIS phase shift $\boldsymbol{\theta}^{(t)}$;
4: Implement Algorithm 1 to obtain the optimal STAR-RIS phase shifts variables $\boldsymbol{\theta}^{(t+1)}$ from the beamforming vector $\mathbf{w}^{(t+1)}$;
5: Calculate $P_T^{(t+1)}$ based on the optimal variables $\boldsymbol{\theta}^{(t+1)}$ and $\mathbf{w}^{(t+1)}$;
6: Update $t = t + 1$;
7: **end while**
8: **Output**: optimal solutions of $\boldsymbol{\theta}^*$ and $\mathbf{w}^*$ and the maximized total achievable rate P_T^*.

IV. Proposed QAOA solution for the total signal power maximization problem in the case of $Q = 2$

Following from Section III, the reformulated problem can be expressed as follows:

$$\max_{\mathbf{w},\boldsymbol{\theta}} \; P_T(\mathbf{w}, \boldsymbol{\theta}), \tag{23a}$$

$$\text{s.t. } \|\mathbf{w}\|^2 = P_{\max}, \tag{23b}$$

$$\|\mathbf{w_n}\|^2 \geq P_{\min}, \tag{23c}$$

$$\theta_p \in \mathcal{D}_2, \forall p \in \mathcal{P}, \tag{23d}$$

where $\mathcal{D}_2 = \{0, \pi/2, \pi, 3\pi/2\}$. The key distinction is that the number of phase shifts expands from two values $\mathcal{D}_1$ to $\mathcal{D}_2$, meaning that $\sin\theta$ is not always equal to 0. However, the stages of solving this problem are still identical to those in Section III, and we only need to handle the different phase shift subproblem. Equivalently, this subproblem can be formulated as follows:

$$\min_{\boldsymbol{\theta}} \; -P_{T,\boldsymbol{\theta}}^{(t)}(\boldsymbol{\theta}), \tag{24a}$$

$$\text{s.t. } \theta_p \in \mathcal{D}_2, \forall p \in \mathcal{P}. \tag{24b}$$

As we know, the objective can be rewritten as (7). The procedure continues by setting $e^{j\theta} = \cos\theta + j\sin\theta$, and the term $Q_{n,\boldsymbol{\theta}}^{(t)}(\boldsymbol{\theta})$ can be reformulated as

$$\begin{aligned} Q_{n,\boldsymbol{\theta}}^{(t)}(\boldsymbol{\theta}) = \Bigg(\sum_{m\in\mathcal{M}} \sum_{p\in\mathcal{P}} (S_{p,nm}^{i,(t)} \cos\theta_p + S_{p,nm}^{r,(t)} \sin\theta_p) \\ + \sum_{m\in\mathcal{M}} T_{nm}^{i,(t)} \Bigg)^2 + \Bigg(\sum_{m\in\mathcal{M}} T_{nm}^{r,(t)} \\ + \sum_{m\in\mathcal{M}} \sum_{p\in\mathcal{P}} (S_{p,nm}^{r,(t)} \cos\theta_p - S_{p,nm}^{i,(t)} \sin\theta_p) \Bigg)^2. \end{aligned} \tag{25}$$

Alternately, (25) can be reduced as

$$\begin{aligned} Q_{n,\boldsymbol{\theta}}^{(t)}(\boldsymbol{\theta}) &= (\mathcal{T}_n^{r,(t)})^2 + (\mathcal{T}_n^{i,(t)})^2 \\ &+ \sum_{p\in\mathcal{P}} \left[(\mathcal{S}_{p,n}^{r,(t)})^2 + (\mathcal{S}_{p,n}^{i,(t)})^2 \right] \\ &+ 2\sum_{p\in\mathcal{P}} \cos\theta_p \mathcal{A}_{p,n}^{(t)} + 2\sum_{p\in\mathcal{P}} \sin\theta_p \mathcal{D}_{p,n}^{(t)} \\ &+ \sum_{\substack{p,q\in\mathcal{P} \\ p\neq q}} (\cos\theta_p \cos\theta_q + \sin\theta_p \sin\theta_q) \mathcal{B}_{pq,n}^{(t)} \\ &+ 2\sum_{p,q\in\mathcal{P}} \cos\theta_p \sin\theta_q \mathcal{E}_{pq,n}^{(t)}, \end{aligned} \tag{26}$$

where $\mathcal{D}_{p,n}^{(t)} = \mathcal{S}_{p,n}^{r,(t)} \mathcal{T}_n^{i,(t)} - \mathcal{S}_{p,n}^{i,(t)} \mathcal{T}_n^{r,(t)}$ and $\mathcal{E}_{pq,n}^{(t)} = \mathcal{S}_{p,n}^{i,(t)} \mathcal{S}_{q,n}^{r,(t)} - \mathcal{S}_{p,n}^{r,(t)} \mathcal{S}_{q,n}^{i,(t)}$. The term $Q_{n,\boldsymbol{\theta}}^{(t)}(\boldsymbol{\theta})$ is now related to $\sin\theta_p$ and $\cos\theta_p$. The next step is to perform them by linear combinations of bits. The discrete phase shifts in $\mathcal{D}_2$ can be illustrated as $\theta_p = (a_p + 2b_p)\pi/2$, where a_p and b_p are bit variables. Following this, the functions $\cos\theta_p$ and $\sin\theta_p$ can be given as

$$\begin{aligned} \sin\theta_p &= a_p(1 - 2b_p), \\ \cos\theta_p &= (1 - a_p)(1 - 2b_p). \end{aligned} \tag{27}$$

However, these linear combinations are suboptimal as the term $a_p b_p$ is quadratic. Substituting it directly into (26) results in a quartic polynomial or a higher-order binary optimization expression, which significantly complexifies the problem. To avoid this, for each $p \in \mathcal{P}$, we denote auxiliary bits c_p that satisfies $c_p = a_p b_p$. To enforce this constraint, we use the penalty function developed in [42] and [43] as

$$g(a_p, b_p, c_p) = \lambda_p(3c_p + a_p b_p - 2a_p c_p - 2b_p c_p), \tag{28}$$

where λ_p is the parameter that impose a penalty on the term $3c_p + a_p b_p - 2a_p c_p - 2b_p c_p$ if they are not equal to zero. Hence, the formulations on (27) can be rewritten as

$$\begin{aligned} \sin\theta_p &= a_p - 2c_p, \\ \cos\theta_p &= 1 - a_p - 2b_p + 2c_p. \end{aligned} \tag{29}$$

The next step is to add the penalty terms from (28) and substitute the linear combinations from (29) to (26) for the QUBO formulation. Since the coefficients do not affect the QUBO optimization problem, they are reduced and we can reduce $Q_{n,\boldsymbol{\theta}}^{(t)}(\boldsymbol{\theta})$ as follows:

$$
\begin{aligned}
&Q^{(t)}_{n,\boldsymbol{\theta}}(\boldsymbol{\theta}) \\
&= \sum_{p\in\mathcal{P}} a_p\Big(-2\mathcal{A}^{(t)}_{p,n} + 2\mathcal{D}^{(t)}_{p,n} + \sum_{\substack{q\in\mathcal{P}\\ q\neq p}}(-2\mathcal{B}^{(t)}_{pq,n} + 2\mathcal{E}^{(t)}_{pq,n})\Big) \\
&+ \sum_{p\in\mathcal{P}} b_p\Big(-4\mathcal{A}^{(t)}_{p,n} - 4\sum_{\substack{q\in\mathcal{P}\\ q\neq p}}\mathcal{B}^{(t)}_{pq,n}\Big) \\
&+ \sum_{p\in\mathcal{P}} c_p\Big(4\mathcal{A}^{(t)}_{p,n} - 4\mathcal{D}^{(t)}_{p,n} + \sum_{\substack{q\in\mathcal{P}\\ q\neq p}}(4\mathcal{B}^{(t)}_{pq,n} + 4\mathcal{E}^{(t)}_{pq,n})\Big) \\
&+ \sum_{\substack{p,q\in\mathcal{P}\\ q\neq p}}\Big[a_pa_q(2\mathcal{B}^{(t)}_{pq,n}) + a_pb_q(4\mathcal{B}^{(t)}_{pq,n} + 4\mathcal{E}^{(t)}_{pq,n}) \\
&\qquad + a_pc_q(-8\mathcal{E}^{(t)}_{pq,n}) + b_pb_q(4\mathcal{B}^{(t)}_{pq,n}) \\
&\qquad + b_pc_q(-8\mathcal{B}^{(t)}_{pq,n} + 8\mathcal{E}^{(t)}_{pq,n}) + c_pc_q(8\mathcal{B}^{(t)}_{pq,n})\Big]. \qquad (30)
\end{aligned}
$$

This formulation can be achieved thanks to the fact that $\mathcal{D}^{(t)}_{p,n} = \mathcal{D}^{(t)}_{qp,n}$ and $\mathcal{E}^{(t)}_{pq,n} = -\mathcal{E}^{(t)}_{pq,n}$. Note that the penalty terms λ_p must be carefully chosen to ensure smooth convergence. Using high penalty values forces the solver to strictly satisfy the constraints, but this rigidity can make the problem difficult to solve and significantly slow down convergence. On the other hand, using low penalty values often allows for faster convergence, but the solver may not be guided strongly enough, risking a final solution that violates the constraints. Thus, a good way to handle this is to set λ_p as an upper bound of the function. It can be seen that the QUBO objective is $-\sum_{n\in\mathcal{N}} Q^{(t)}_{n,\boldsymbol{\theta}}(\boldsymbol{\theta})$ and the upper bound of this formulation can be expressed as follows:

$$
\begin{aligned}
&\lambda_p = \\
&\sum_{\substack{p\in\mathcal{P}\\ n\in\mathcal{N}}} \max\Big\{0, 2\mathcal{A}^{(t)}_{p,n} - 2\mathcal{D}^{(t)}_{p,n} + \sum_{\substack{q\in\mathcal{P}\\ q\neq p}}(2\mathcal{B}^{(t)}_{pq,n} - 2\mathcal{E}^{(t)}_{pq,n})\Big\} \\
&+ \sum_{\substack{p\in\mathcal{P}\\ n\in\mathcal{N}}} \max\Big\{0, 4\mathcal{A}^{(t)}_{p,n} + 4\sum_{\substack{q\in\mathcal{P}\\ q\neq p}}\mathcal{B}^{(t)}_{pq,n}\Big\} \\
&+ \sum_{\substack{p\in\mathcal{P}\\ n\in\mathcal{N}}} \max\Big\{0, -4\mathcal{A}^{(t)}_{p,n} + 4\mathcal{D}^{(t)}_{p,n} - \sum_{\substack{q\in\mathcal{P}\\ q\neq p}}(4\mathcal{B}^{(t)}_{pq,n} + 4\mathcal{E}^{(t)}_{pq,n})\Big\} \\
&+ \sum_{\substack{p,q\in\mathcal{P}\\ q\neq p\\ n\in\mathcal{N}}} \Big[\max\Big\{0, -14\mathcal{B}^{(t)}_{pq,n}\Big\} + \max\Big\{0, -4\mathcal{B}^{(t)}_{pq,n} - 4\mathcal{E}^{(t)}_{pq,n}\Big\} \\
&+ \max\Big\{0, 8\mathcal{E}^{(t)}_{pq,n}\Big\} + \max\Big\{0, 8\mathcal{B}^{(t)}_{pq,n} - 8\mathcal{E}^{(t)}_{pq,n}\Big\}\Big]. \qquad (31)
\end{aligned}
$$

Following this, by taking the negative sum of $Q^{(t)}_{n,\boldsymbol{\theta}}(\boldsymbol{\theta})$ and adding the penalty introduced in (28), the final QUBO formulation can be formulated as follows:

$$
\begin{aligned}
&\mathcal{P}^{(t)}_{\text{QUBO}} \\
&\triangleq -\sum_{n\in\mathcal{N}} Q^{(t)}_{n,\boldsymbol{\theta}}(\boldsymbol{\theta}) + \sum_{p\in\mathcal{P}} \lambda_p(3c_p + a_pb_p - 2a_pc_p - 2b_pc_p). \\
&= \sum_{p\in\mathcal{P}}\Big\{a_p\sum_{n\in\mathcal{N}}\Big(2\mathcal{A}^{(t)}_{p,n} - 2\mathcal{D}^{(t)}_{p,n} + \sum_{\substack{q\in\mathcal{P}\\ q\neq p}}(2\mathcal{B}^{(t)}_{pq,n} + 2\mathcal{E}^{(t)}_{pq,n})\Big) \\
&+ b_p\sum_{n\in\mathcal{N}}\Big(4\mathcal{A}^{(t)}_{p,n} + 4\sum_{\substack{q\in\mathcal{P}\\ q\neq p}}\mathcal{B}^{(t)}_{pq,n}\Big) \\
&+ c_p\Big[\sum_{n\in\mathcal{N}}\Big(-4\mathcal{A}^{(t)}_{p,n} + 4\mathcal{D}^{(t)}_{p,n} + \sum_{\substack{q\in\mathcal{P}\\ q\neq p}}(-4\mathcal{B}^{(t)}_{pq,n} - 4\mathcal{E}^{(t)}_{pq,n})\Big) \\
&+ 3\lambda_p\Big] + a_pb_p\lambda_p - 2a_pc_p\lambda_p - 2b_pc_p\lambda_p\Big\} \\
&+ \sum_{\substack{p,q\in\mathcal{P}\\ q\neq p}}\Big[2a_pa_q\mathcal{B}^{(t)}_{pq,n} - a_pb_q(4\mathcal{B}^{(t)}_{pq,n} + 4\mathcal{E}^{(t)}_{pq,n}) + 8a_pc_q\mathcal{E}^{(t)}_{pq,n} \\
&+ 4b_pb_q\mathcal{B}^{(t)}_{pq,n} + b_pc_q(8\mathcal{B}^{(t)}_{pq,n} - 8\mathcal{E}^{(t)}_{pq,n}) - 8c_pc_q\mathcal{B}^{(t)}_{pq,n}\Big]. \qquad (32)
\end{aligned}
$$

Having obtained the formulation for the QUBO, we now construct the minimization problem with the variable vector $\mathbf{x} = [\mathbf{a}, \mathbf{b}, \mathbf{c}]^T$, where $\mathbf{a}, \mathbf{b}, \mathbf{c}$ are $\{0,1\}^{1\times P}$ vectors which contain the corresponding sets of variables a_p, b_p, c_p, respectively. The $\mathbf{Q}$-matrix can be constructed as

$$
\mathbf{Q} = \begin{pmatrix} \mathbf{Q}^{(\mathbf{aa})} & \mathbf{Q}^{(\mathbf{ab})} & \mathbf{Q}^{(\mathbf{ac})} \\ \left(\mathbf{Q}^{(\mathbf{ab})}\right)^T & \mathbf{Q}^{(\mathbf{bb})} & \mathbf{Q}^{(\mathbf{bc})} \\ \left(\mathbf{Q}^{(\mathbf{ac})}\right)^T & \left(\mathbf{Q}^{(\mathbf{bc})}\right)^T & \mathbf{Q}^{(\mathbf{cc})} \end{pmatrix}. \qquad (33)
$$

Herein, $\mathbf{Q}^{(\mathbf{uv})}, \mathbf{u}, \mathbf{v} \in \{\mathbf{a}, \mathbf{b}, \mathbf{c}\}$ is the submatrix that represents the vector variables $\mathbf{u}$ horizontally and $\mathbf{v}$ vertically. The components of these matrices at the p-th row and q-th column can be denoted as $Q^{(\mathbf{uv})}_{p,q}$ and as shown in (30), their values can be given as

$$
\begin{aligned}
Q^{(\mathbf{aa})}_{p,q} &= \begin{cases} 2\sum_{n\in\mathcal{N}}\sum_{\substack{q\in\mathcal{P}\\ q\neq p}}\mathcal{B}^{(t)}_{pq,n}, & p\neq q, \\ \sum_{n\in\mathcal{N}}\Big(2\mathcal{A}^{(t)}_{p,n} - 2\mathcal{D}^{(t)}_{p,n} \\ \quad + \sum_{\substack{q\in\mathcal{P}\\ q\neq p}}(2\mathcal{B}^{(t)}_{pq,n} + 2\mathcal{E}^{(t)}_{pq,n})\Big), & p = q, \end{cases} \\
Q^{(\mathbf{ab})}_{p,q} &= \begin{cases} \sum_{n\in\mathcal{N}}\sum_{\substack{q\in\mathcal{P}\\ q\neq p}}\Big(-4\mathcal{B}^{(t)}_{pq,n} - 4\mathcal{E}^{(t)}_{pq,n}\Big), & p\neq q, \\ \lambda_p, & p = q, \end{cases} \\
Q^{(\mathbf{ac})}_{p,q} &= \begin{cases} 8\sum_{n\in\mathcal{N}}\sum_{\substack{q\in\mathcal{P}\\ q\neq p}}\mathcal{B}^{(t)}_{pq,n}, & p\neq q, \\ -2\lambda_p, & p = q, \end{cases} \\
Q^{(\mathbf{bb})}_{p,q} &= \begin{cases} 4\sum_{n\in\mathcal{N}}\sum_{\substack{q\in\mathcal{P}\\ q\neq p}}\mathcal{B}^{(t)}_{pq,n}, & p\neq q, \\ \sum_{n\in\mathcal{N}}\Big(4\mathcal{A}^{(t)}_{p,n} + 4\sum_{\substack{q\in\mathcal{P}\\ q\neq p}}\mathcal{B}^{(t)}_{pq,n}\Big), & p = q, \end{cases} \\
Q^{(\mathbf{bc})}_{p,q} &= \begin{cases} \sum_{n\in\mathcal{N}}\sum_{\substack{q\in\mathcal{P}\\ q\neq p}}\Big(8\mathcal{B}^{(t)}_{pq,n} - 8\mathcal{E}^{(t)}_{pq,n}\Big), & p\neq q, \\ -2\lambda_p, & p = q, \end{cases} \\
Q^{(\mathbf{cc})}_{p,q} &= \begin{cases} -8\sum_{n\in\mathcal{N}}\sum_{\substack{q\in\mathcal{P}\\ q\neq p}}\mathcal{B}^{(t)}_{pq,n} & p\neq q, \\ \sum_{n\in\mathcal{N}}\Big(-4\mathcal{A}^{(t)}_{p,n} + 4\sum_{p\in\mathcal{P}}\mathcal{D}^{(t)}_{p,n} \\ \quad + \sum_{\substack{q\in\mathcal{P}\\ q\neq p}}(-4\mathcal{B}^{(t)}_{pq,n} - 4\mathcal{E}^{(t)}_{pq,n})\Big) + 3\lambda_p, & p = q. \end{cases} \qquad (34)
\end{aligned}
$$

In order to convert the QUBO formulation in (30) to the Hamiltonian form, we denote the spin variables $z_{x_p} = 1 - 2x_p, \forall x \in \{a, b, c\}, p \in \mathcal{P}$ and get the reformulation $x_p = \frac{1-z_{x_p}}{2}, \forall x \in \{a, b, c\}, p \in \mathcal{P}$. The final Hamiltonian can be obtained by substituting these equations directly into (32) and expressed as follows:

$$
\begin{aligned}
&H_{\text{final}}^{(t)} \\
&= \sum_{p\in\mathcal{P}} \Bigg[z_{a_p} \Bigg(\sum_{n\in\mathcal{N}} (-\mathcal{A}_{p,n}^{(t)} + \mathcal{D}_{p,n}^{(t)} - \sum_{\substack{q\neq p \\ q\in\mathcal{P}}} 3\mathcal{B}_{pq,n}^{(t)}) + \frac{\lambda_p}{4} \Bigg) \\
&+ z_{b_p} \Bigg(\sum_{n\in\mathcal{N}} (-2\mathcal{A}_{p,n}^{(t)} + \sum_{\substack{q\neq p \\ q\in\mathcal{P}}} (-5\mathcal{B}_{pq,n}^{(t)} + \mathcal{E}_{pq,n}^{(t)})) + \frac{\lambda_p}{4} \Bigg) \\
&+ z_{c_p} \Bigg(\sum_{n\in\mathcal{N}} (2\mathcal{A}_{p,n}^{(t)} - 2\mathcal{D}_{p,n}^{(t)} + \sum_{\substack{q\neq p \\ q\in\mathcal{P}}} 2\mathcal{B}_{pq,n}^{(t)}) \Bigg) - \frac{\lambda_p}{2} \Bigg) \\
&+ \sum_{n\in\mathcal{N}} \left(z_{a_p} z_{b_p} \frac{\lambda_p}{4} - z_{a_p} z_{c_p} \frac{\lambda_p}{2} - z_{b_p} z_{c_p} \frac{\lambda_p}{2} \right) \Bigg] \\
&+ \sum_{\substack{q\neq p \\ q\in\mathcal{P}}} \sum_{n\in\mathcal{N}} \Bigg[z_{a_p} z_{a_q} \frac{\mathcal{B}_{pq,n}^{(t)}}{2} - z_{a_p} z_{b_q} (\mathcal{B}_{pq,n}^{(t)} + \mathcal{E}_{pq,n}^{(t)}) \\
&\qquad + 2 z_{a_p} z_{c_q} \mathcal{B}_{pq,n}^{(t)} + z_{b_p} z_{b_q} \mathcal{B}_{pq,n}^{(t)} \\
&\qquad + z_{b_p} z_{c_q} (2\mathcal{B}_{pq,n}^{(t)} - 2\mathcal{E}_{pq,n}^{(t)}) - 2 z_{c_p} z_{c_q} \mathcal{B}_{pq,n}^{(t)} \Bigg]. \qquad (35)
\end{aligned}
$$

After solving the phase shifts subproblem by QAOA, the optimized phase shifts are substituted to the primary objective to attain the new objective $P_{T,\mathbf{w}}^{(t)}$ of the beamforming optimization subproblem. This subproblem is subsequently solved by following the methodology outlined in Section III-B. The algorithm applied is Algorithm 2 where the factors are alternatively optimized until convergence or the maximum number of iterations is reached.

V. Simulation Results and Discussions

A. Simulation Settings

In this section, we present the results of extensive simulations to verify the proposed algorithm. For the simulations, the number of antennas used at the BS was set to $M = 8$, while the number of terrestrial users was $N = 3$. Without loss of generality, the location of the terrestrial BS was set to be $[0, 0, 50]$ meters, while the terrestrial users had their positions fixed at $[100, 50, 0]$, $[180, -40, 0]$ and $[-75, 120, 0]$ meters, respectively. The location of the center of the STAR-RIS center was assumed to be $[75, 50, 20]$. The maximum power broadcast by the BS was set to 40 dBm, and the minimum power allocated to each user was 27 dBm. In addition, the path loss exponents of different channel types set at $\varphi_i = 2.2, \varphi_r = 2.6, \varphi_d = 3.5$, and the noise power $\sigma^2 = -90$dBm. The number of qubits used in the optimization problem was configured to be in the range of $[3, 18]$, while the number of random Rayleigh channels simulated in this work is 50.

Since our proposed optimization problem is discretized into binary variables associated with phases, the number of qubits we have to handle for each case varies differently. In the case where the number of phases in set $\mathcal{D}_Q$ is 2, i.e., $Q = 1$, the number of qubits a_p formed in the QUBO expression is equal to the number of STAR-RIS elements P. However, in the case of $Q = 2$, the number of qubits increases to a_p, b_p and c_p for each STAR-RIS element p. This significantly increases the number of qubits to $3P$. The simulations were performed in Python using the simulation libraries as `qiskit, qiskit_aer` and `qiskit_algorithms`. For the optimizer used in QAOA, we use COBYLA with default settings in `qiskit` library, whereas the initial parameters of $(\boldsymbol{\gamma}, \boldsymbol{\beta})$ are randomized in $[0, \pi/2]$. The number of layers used in our QAOA model is $M_Q = 1$.

B. Numerical Results and Discussions

In both Figs. 3a and 3b, we can observe that the convergence curve of the QUBO objective is overwhelmingly flat as the number of qubits increases. Although the angles $\boldsymbol{\gamma}, \boldsymbol{\beta}$ are repeatedly updated by the classical COBYLA optimizer, the landscapes of the multiple-qubit QUBO objectives remain almost flat. This behavior might be caused by the barren plateau problem in variational quantum computing [44], [45]. Mathematically, the variance of the cost function in parameterized quantum circuits decreases exponentially with the number of qubits. Consequently, the cost function gradient is close to zero, yielding an almost flat QUBO landscape and making the problem harder to train. Thus, barren plateaus represent one of the main challenges in training quantum circuits, and their mitigation will be a key focus of our future work to enhance trainability in larger systems.

Figs. 4(a) and 4(b) represent the QAOA-AO convergence in all AO iterations for 18 qubits. In general, each AO loop takes around 25 iterations to converge, in which the first 20 iterations are used in the exploration phase. After looking for the minimum value of the QUBO objective and achieving the new optimized phase shift $\boldsymbol{\theta}^{(1)}$, the optimized BS beamforming $\mathbf{w}^{(1)}$ is attained by the direct solution. Then, Algorithm 1 is utilized again to derive the better optimized phase shift $\boldsymbol{\theta}^{(2)}$ from the newly optimized beamforming $\mathbf{w}^{(1)}$ in the BS. In both Figs. 4a and 4b, the minimized values of the second AO loop are lower than those of the first AO loop, which shows that the proposed AO algorithm works well for a relatively high number of qubits.

Figs. 5(a) and 5(b) depict the improvement in total transmission power to ground users in the STAR-RIS-aided wireless networks. In particular, the Beam Opt results are given by only optimizing the beamforming vectors of the initial feasible points while keeping the phase shifts fixed, as demonstrated in Section III-B. Theoretically, the AO algorithm ensures that the solution converges at a local optimum point; therefore, the performance of the AO algorithm might be lower than the exhaustive search, since they always derive the global optimum point. However, the numerical results of these two approaches are quite close. Moreover, the performance of the QAOA-AO method is superior to that of the only optimizing beamforming method, which validates the efficiency of the proposed method. When deploying a STAR-RIS with a fixed number of reflecting elements, it is widely known that using a quadrature quantization phase set ($Q = 2, \mathcal{D}_2 = \{0, \pi/2, \pi, 3\pi/2\}$) typically

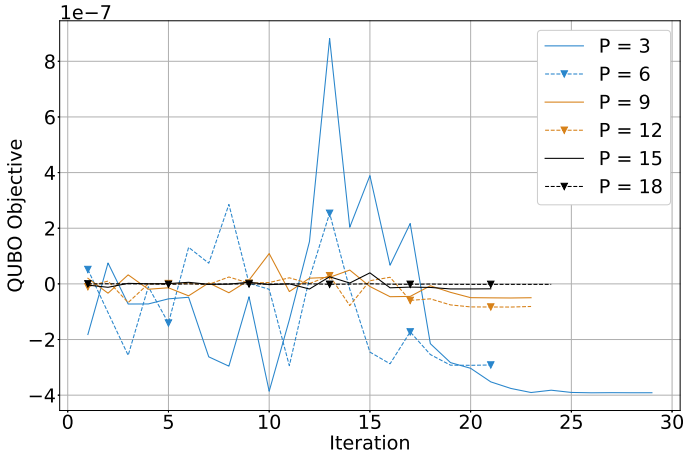

(a)

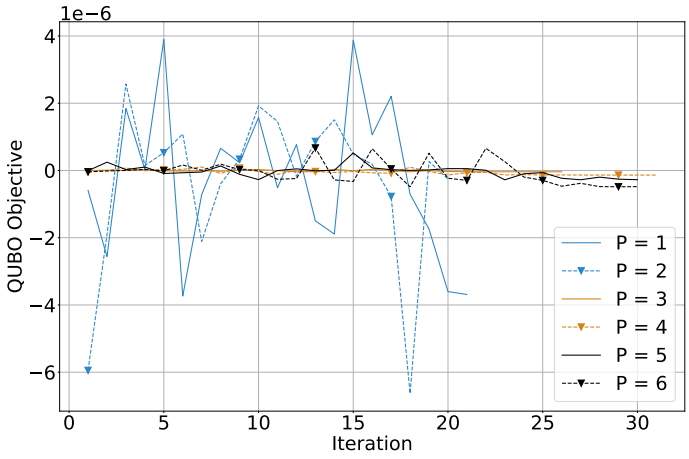

(b)

Fig. 3: Convergence behavior of Algorithm 1 in the same DL channel, regarding the last AO iteration with multiple qubits ranging from $[3, 18]$. (a) The $Q = 1$ case, (b) The $Q = 2$ case.

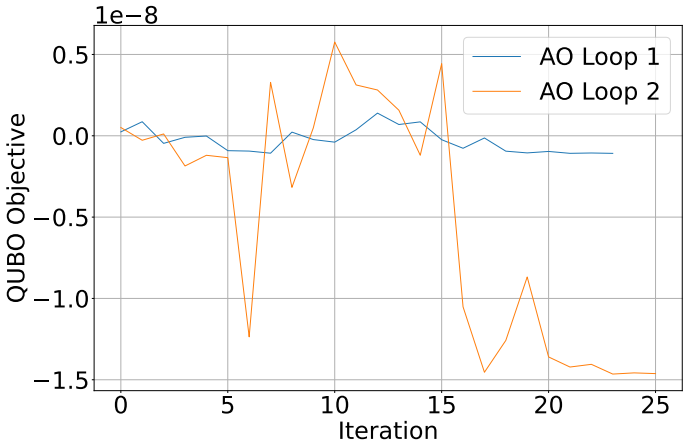

(a)

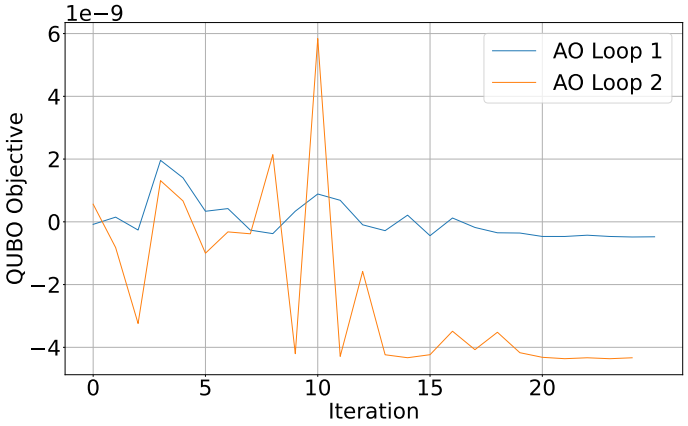

(b)

Fig. 4: Convergence behavior of the QUBO objective function across the first two AO iterations in the 18-qubit case. (a) The $Q = 1$ case, (b) The $Q = 2$ case.

outperforms binary phase quantization ($Q = 1, \mathcal{D}_1 = \{0, \pi\}$). Nevertheless, in this study, both quantization schemes share the same qubit budget, such that the number of RIS elements controllable in the $Q = 1$ case is three times greater than in the $Q = 2$ case. In both quantization scenarios ($Q = 1$ and $Q = 2$), the total power transmitted from the BS to the users is substantially higher for $Q = 1$ than for $Q = 2$ when normalized to the same qubit budget. This result indicates that with the limitation of the number of qubits used in real quantum computers or simulators, allocating qubits to achieve finer phase resolution ($Q = 2$) across fewer RIS elements is less effective than distributing them to control a larger number of RIS elements with coarser phase quantization $Q = 1$.

Fig. 6 demonstrates the difference in the average iterations of the QAOA-AO algorithm in the $Q = 1$ and $Q = 2$ cases. Each AO run requires a minimum of two iterations, as the final iteration is reserved for verifying the convergence condition. Notably, as the number of qubits increases, the average number of iterations needed for QAOA-AO to converge increases gradually, though this growth rate diminishes at higher qubit counts. Importantly, the iterations taken in the case $Q = 1$ is higher than those in the case $Q = 2$, mainly because the QUBO formulation of the case $Q = 2$ is affected by the penalty component λ_p. Since the value of λ_p is carefully chosen to be much larger than the range of values of the constraint objective $\sum_{n\in\mathcal{N}} Q^{(t)}_{n,\boldsymbol{\theta}}(\boldsymbol{\theta})$, the exploration phase of the QAOA algorithm can quickly eliminate infeasible points. Moreover, the penalty λ_p only affects the linear and some of the quadratic terms of the QUBO expression, creating a vital imbalance between the quadratic terms and the linear terms, so that the QAOA optimization process can focus on the most valuable components of the expression.

Figs. 7(a) and 7(b) show the exponential growth of the runtime ratio between the QAOA-AO and the brute force approaches, considering the same increase in the number of qubits from 6 to 18 qubits. The runtime for each N-qubit scenario is normalized by the runtime of the 3-qubit case. In both figures, the time ratio from the brute force approach is enormous compared to the time ratio of the QAOA-AO method. Additionally, the brute-force runtime grows significantly faster than QAOA-AO as qubit count increases. This result also validates the robustness of the proposed QAOA-AO

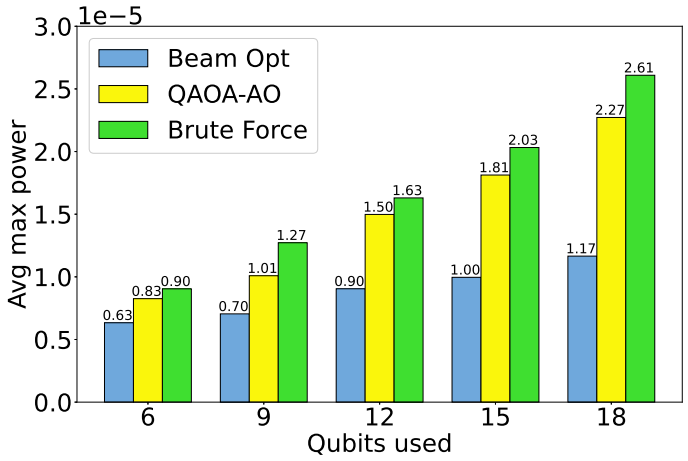

(a)

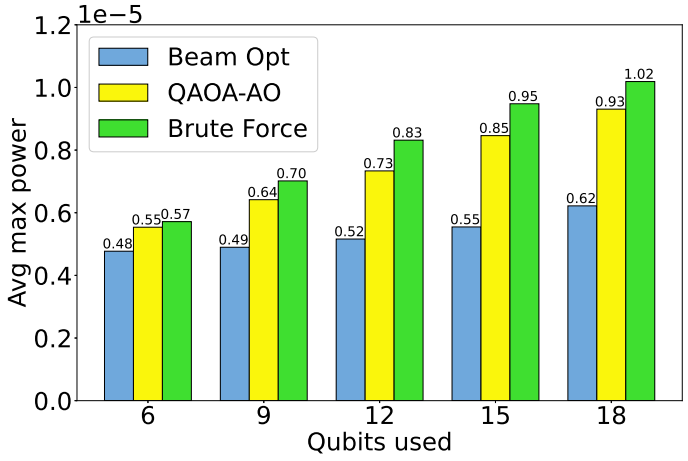

(b)

Fig. 5: Enhancement of total power transmitted from BS to users with the help of STAR-RIS. (a) The $Q = 1$ case, (b) The $Q = 2$ case.

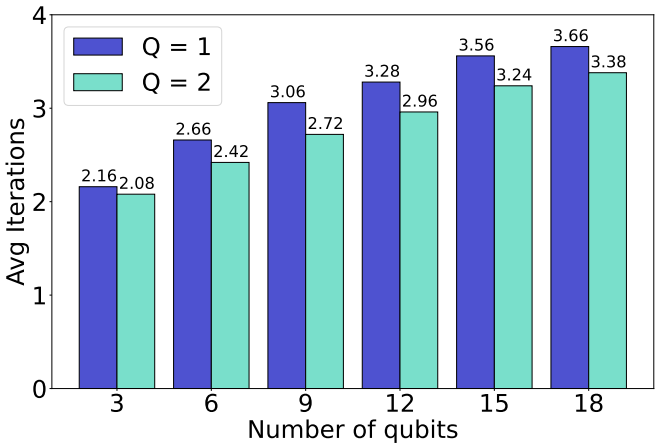

Fig. 6: Comparison of average iteration taken by QAOA-AO algorithm applied in $Q = 1$ and $Q = 2$ cases for qubits in range $[3, 18]$.

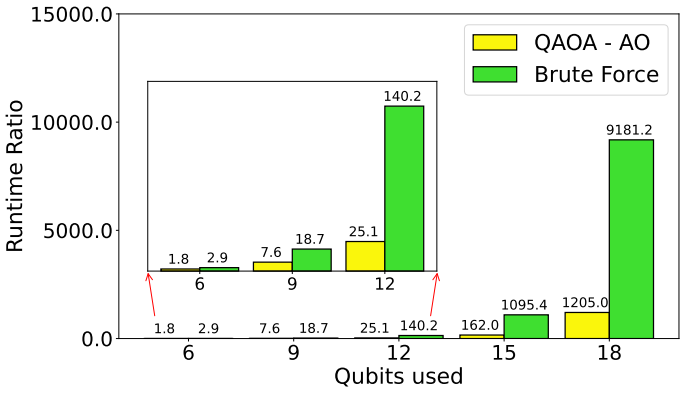

(a)

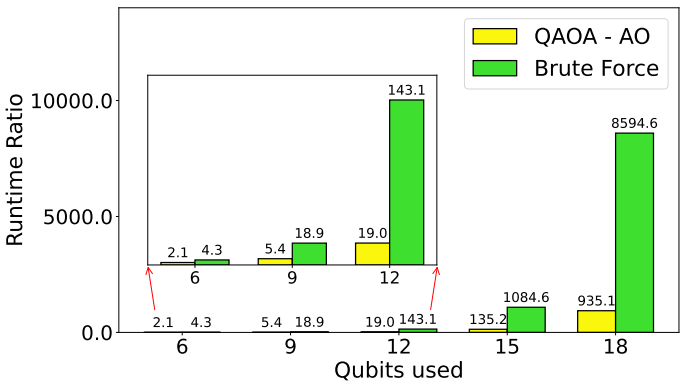

(b)

Fig. 7: The time ratio of QAOA-AO algorithm compared with brute force at two $Q = 1$ and $Q = 2$ for qubits in range $[6, 18]$. (a) The $Q = 1$ case, (b) The $Q = 2$ case.

method and further validates the potential that the operation time of the hybrid quantum-classical methods can be much smaller than the classical computing, especially for intractable or NP-hard problems involving a large number of qubits.

VI. Conclusion

In this paper, we have investigated the integrated challenge of addressing the STAR-RIS optimization problem using quantum computing by proposing the AO-based framework. The proposed QAOA-AO method has been employed to decompose the original problem into two parts: a phase subproblem, tackled with a QAOA-based algorithm, and a beamforming subproblem, which is solved by a closed-form expression. Numerical solutions demonstrate that our proposed QAOA-AO method generally surpasses classical exhaustive search in runtime efficiency for sophisticated problems which seem classically intractable. The QAOA-AO algorithm also achieves near-optimal solutions compared to the brute force method and outperforms the beam optimization-only method. These findings have demonstrated the strong potential of hybrid quantum-classical approaches in handling discrete phase shift STAR-RIS problems, which is more practical than those of continuous phase shift. Looking ahead, future work could explore more advanced quantum-classical hybrid techniques—such as adaptive variational algorithms and BP mitigation strategies—to enhance both the performance and scalability of quantum optimization for STAR-RIS phase design.

REFERENCES

[1] B. Zheng, C. You, W. Mei, and R. Zhang, "A survey on channel estimation and practical passive beamforming design for intelligent reflecting surface aided wireless communications," *IEEE Commun. Surveys Tuts.*, vol. 8, pp. 45 913–45 923, Feb. 2022.

[2] C. Pan, G. Zhou, K. Zhi, S. Hong, T. Wu, and Y. Pan, "An overview of signal processing techniques for RIS/IRS-aided wireless systems," *IEEE J. Sel. Topics Signal Process.*, vol. 16, no. 5, pp. 883–917, Aug. 2022.

[3] A. Cao, T. Ni, Y. Chen, L. Wang, Z. Li, X. Bai, F. Zhang, and Z. Chen, "Conformal radiation-type programmable metasurface for agile millimeter-wave orbital angular momentum generation," *Research.*, vol. 8, Jan. 2025.

[4] R. Liu, Q. Wu, M. D. Renzo, and Y. Yuan, "A path to smart radio environments: An industrial viewpoint on reconfigurable intelligent surfaces," *IEEE Wireless Commun. Mag.*, vol. 29, no. 1, pp. 202–208, Jan. 2022.

[5] H. Yang, X. Cao, F. Yang, J. Gao, S. Xu, M. Li, X. Chen, Y. Zhao, Y. Zheng, and S. Li, "A programmable metasurface with dynamic polarization, scattering and focusing control," *Sci. Rep.*, vol. 6, pp. 1–11, Jul. 2016.

[6] X. Yuan, Y.-J. A. Zhang, Y. Shi, W. Yan, and H. Liu, "Reconfigurable-intelligent-surface empowered wireless communications: Challenges and opportunities," *IEEE Wireless Commun. Mag.*, vol. 28, no. 2, pp. 136–143, Feb. 2021.

[7] Q. Wu and R. Zhang, "Intelligent reflecting surface enhanced wireless network: Joint active and passive beamforming design," in *Proc. 2018 IEEE Global Commun. Conf. (GLOBECOM)*, Abu Dhabi, United Arab Emirates, Dec.9–13 2018.

[8] S. Chaudhary, A. Nehra, I. Budhiraja, R. Chaudhary, and A. Bansal, "STAR-RIS based resource scheduling and mode selection for drone assisted 5G communications," in *IEEE INFOCOM Wksps 2024*, ALondon, United Kingdom, May19–22 2024.

[9] S. Chaudhary, I. Budhiraja, R. Chaudhary, N. Kumar, D. Garg, and A. M. Almuhaideb, "Quantum federated reinforcement-learning-based joint mode selection and resource allocation for STAR-RIS-aided VRCS," *IEEE Internet Things J.*, vol. 11, no. 22, pp. 36 242–36 256, Nov. 2024.

[10] L. Dai, B. Wang, M. Wang, X. Yang, J. Tan, and S. Bi, "Reconfigurable intelligent surface-based wireless communications: Antenna design, prototyping, and experimental results," *IEEE Access*, vol. 28, no. 2, pp. 136–143, Feb. 2020.

[11] L. Y. Y. Y. M. O. H. M.-S. Alouini, "Coverage, probability of SNR gain, and DOR analysis of RIS-aided communication systems," *IEEE Wireless Commun. Lett.*, vol. 9, no. 8, pp. 1268–1272, Apr. 2020.

[12] S. Zeng, H. Zhang, B. Di, Z. Han, and L. Song, "Reconfigurable intelligent surface RIS assisted wireless coverage extension: RIS orientation and location optimization," *IEEE Commun. Lett.*, vol. 25, no. 1, pp. 269–273, Sep. 2020.

[13] C. Wu, Y. Liu, X. Mu, X. Gu, and O. A. Dobre, "Coverage characterization of STAR-RIS networks: NOMA and OMA," *IEEE Commun. Lett.*, vol. 25, no. 9, pp. 3036–3040, Jun. 2021.

[14] X. Wei, D. Shen, and L. Dai, "Channel estimation for RIS assisted wireless communications—Part I: Fundamentals, solutions, and future opportunities," *IEEE Commun. Lett.*, vol. 25, no. 5, pp. 1398–1402, Jan. 2021.

[15] X. Tang, D. Wang, R. Zhang, Z. Chu, and Z. Han, "Jamming mitigation via aerial reconfigurable intelligent surface: Passive beamforming and deployment optimization," *IEEE Trans. Veh. Technol.*, vol. 70, no. 6, pp. 6232–6237, May 2021.

[16] W. Wu, H. Wang, W. Wang, and R. Song, "Doppler mitigation method aided by reconfigurable intelligent surfaces for high-speed channels," *IEEE Wireless Commun. Lett.*, vol. 11, no. 3, pp. 627–631, Dec. 2021.

[17] A. Elzanaty, A. Guerra, F. Guidi, and M.-S. Alouini, "Reconfigurable intelligent surfaces for localization: Position and orientation error bounds," *IEEE Trans. Signal Process.*, vol. 69, pp. 5386–5402, Aug. 2021.

[18] R. Liu, M. Li, H. Luo, Q. Liu, and A. L. Swindlehurst, "Integrated sensing and communication with reconfigurable intelligent surfaces: Opportunities, applications, and future directions," *IEEE Wireless Commun.*, vol. 30, no. 1, pp. 50–57, Mar. 2023.

[19] Z. Chen, K. Wang, J. Li, X. Y. Zhang, and K.-K. Wong, "Large language model-based gray wolf optimization for near-field ISAC networks," *IEEE Trans. Mob. Comput.*, Feb. 2026.

[20] L. Bariah, L. Mohjazi, H. Abumarshoud, B. Selim, S. Muhaidat, and M. Tatipamula, "RIS-assisted space-air-ground integrated networks: New horizons for flexible access and connectivity," *IEEE Netw.*, vol. 37, no. 3, pp. 118–125, Sep. 2022.

[21] P. Mamillapalli, S. Verma, T. K. Rodrigues, and A. Kumar, "Deep reinforcement learning for interference suppression in RIS-aided space-air-ground integrated networks," *arXiv preprint arXiv:2602.06982*, Jan. 2026.

[22] N. DOCOMO. (2020, Jan.) DOCOMO conducts world's first successful trial of transparent dynamic metasurface. [Online]. Available: https://www.docomo.ne.jp/english/info/media_center/pr/2020/0117_00.html

[23] Y. Liu, X. Mu, J. Xu, R. Schober, Y. Hao, and H. V. Poor, "STAR: Simultaneous transmission and reflection for 360° coverage by intelligent surfaces," *IEEE Wireless Commun.*, vol. 28, no. 6, pp. 102–109, Dec. 2021.

[24] J. Xu, Y. Liu, X. Mu, and O. A. Dobre, "STAR-RISs: Simultaneous transmitting and reflecting reconfigurable intelligent surfaces," *IEEE Commun. Lett.*, vol. 25, no. 9, pp. 3134–3138, May 2021.

[25] S. Zhang, W. Hao, G. Sun, C. Huang, Z. Zhu, and X. Li, "Joint beamforming optimization for active STAR-RIS-assisted ISAC systems," *IEEE Trans. Wireless Commun.*, vol. 23, no. 11, pp. 15 888–15 902, Aug. 2024.

[26] L. Liu, B. Ai, Y. Niu, Z. Han, N. Wang, and Z. Ma, "STAR-RIS assisted train-to-ground communications in space-air-ground integrated networks," *IEEE Trans. Commun.*, May 2025.

[27] D. Pepe and D. Zito, "A novel phase shifter for 60 GHz phased arrays," in *2015 26th Signal Syst. Conf. (ISSC)*, Carlow, Ireland, Jun.24-25 2015.

[28] Q. Wu and R. Zhang, "Beamforming optimization for wireless network aided by intelligent reflecting surface with discrete phase shifts," *IEEE Trans. Wireless Commun.*, vol. 68, no. 3, pp. 1838–1851, Dec. 2019.

[29] J.-C. Chen, "Designing STAR-RIS-assisted wireless systems with coupled and discrete phase shifts: A computationally efficient algorithm," *IEEE Trans. Veh. Technol.*, vol. 73, no. 7, pp. 10 772–10 777, Feb. 2024.

[30] R. Zhong, Y. Liu, X. Mu, Y. Chen, X. Wang, and L. Hanzo, "Hybrid reinforcement learning for STAR-RISs: A coupled phase-shift model based beamformer," *IEEE J. Sel. Areas Commun.*, vol. 40, no. 9, pp. 2556–2569, Jul. 2022.

[31] E. Farhi, J. Goldstone, and S. Gutmann, "A quantum approximate optimization algorithm," *arXiv preprint arXiv:1411.4028*, 2014.

[32] J. Preskill, "Quantum computing in the NISQ era and beyond," *Quantum*, vol. 2, p. 79, Aug. 2018.

[33] Qiskit. (2018, Dec.) Introducing qiskit aer: A high performance simulator framework for quantum circuits. [Online]. Available: https://medium.com/qiskit/qiskit-aer-d09d0fac7759

[34] U. Azad, B. K. Behera, E. A. Ahmed, P. K. Panigrahi, and A. Farouk, "Solving vehicle routing problem using quantum approximate optimization algorithm," *IEEE Trans. Intell. Transp. Syst.*, vol. 24, no. 7, pp. 7564–7573, May 2022.

[35] K. Kea, C. Huot, and Y. Han, "Leveraging knapsack QAOA approach for optimal electric vehicle charging," *IEEE Access.*, vol. 11, pp. 109 964–109 973, Sep. 2023.

[36] R. Mahroo and A. Kargarian, "Learning infused quantum-classical distributed optimization technique for power generation scheduling," *IEEE Trans. Quantum Eng.*, vol. 4, pp. 1–14, Sep. 2023.

[37] V. P. Pham, D. V. Huynh, E. Ak, L. D. Nguyen, B. Canberk, O. A. Dobre, and T. Q. Duong, "Joint optimal design for speed and routing in maritime logistics for green supply chain: A quantum approximate optimization algorithm approach," *IEEE Internet Things J.*, vol. 12, no. 19, pp. 39 556–39 571, 2025.

[38] D. V. Huynh, O. A. Dobre, and T. Q. Duong, "Optimal service placement for 6G edge computing with quantum-centric optimization in real quantum hardware," *IEEE Commun. Lett.*, vol. 29, no. 3, pp. 448–452, Dec. 2024.

[39] Q. Wu and R. Zhang, "Towards smart and reconfigurable environment: Intelligent reflecting surface aided wireless network," *IEEE Commun. Mag.*, vol. 58, no. 1, pp. 106–112, Nov. 2019.

[40] M.-M. Zhao, Q. Wu, M.-J. Zhao, and R. Zhang, "IRS-aided wireless communication with imperfect CSI: Is amplitude control helpful or not?" in *Proc. 2020 IEEE Global Commun. Conf. (GLOBECOM)*, Taipei, Taiwan, Dec. 2020.

[41] Y. Saad, *Numerical Methods for Large Eigenvalue Problems: Revised Edition*, 2nd ed. Society for Industrial & Applied Mathematics, U.S., 2011.

[42] R. Babbush, B. O'Gorman, and A. Aspuru-Guzik, "Resource efficient gadgets for compiling adiabatic quantum optimization problems," *Annalen der Physik*, vol. 525, no. 10–11, pp. 877–888, Sep. 2013.

[43] J. D. Biamonte, "Nonperturbative k-body to two-body commuting conversion hamiltonians and embedding problem instances into ising spins," *Phys. Rev. A*, vol. 77, p. 052331, May 2008.

[44] G. Stenzel, T. Rohe, M. Kölle, L. Sünkel, J. Stein, and C. Linnhoff-Popien, "Illustration of barren plateaus in quantum computing," *arXiv preprint arXiv:2602.16558*, 2026.

[45] M. Larocca, S. Thanasilp, S. Wang, K. Sharma, J. Biamonte, P. J. Coles, L. Cincio, J. R. McClean, Z. Holmes, and M. Cerezo, "Illustration of barren plateaus in quantum computing," *Nat Rev Phys 7*, pp. 174—189, Mar. 2025.